AVO crossplot analysis in unconsolidated sediments containing gas hydrate and free gas: Green Canyon 955, Gulf of Mexico

Zijian Zhang[1], Daniel R. McConnell[1], De-hua Han[2]*
[1]Fugro GeoConsulting, Inc., and [2]Rock Physics Lab, University of Houston

Summary

An analysis of amplitude variation with offset (AVO) observations is applied in hydrate-bearing sands, free-gas-charged sands, and hydrate-over-gas sands. The elastic model parameters (Vp, Vs, and density) are obtained from well log measurements and a rock physics model. The study suggests that presence of gas hydrate and free gas affect the AVO of shallow unconsolidated sediments containing gas hydrate and free gas. Low-concentrated gas hydrate and low-concentrated gas hydrate overlying free gas have weak AVO behaviors while highly-concentrated gas hydrate and highly-concentrated gas hydrate overlying free gas have strong AVO behaviors. Both highly-concentrated gas hydrate and highly-concentrated gas hydrate overlying free gas are Class I AVO anomalies but the intercept of AVO is stronger negative for highly-concentrated gas hydrate overlying free gas. They may occur in different locations in the AVO intercept and gradient plane.

Introduction

Shallow gas and gas hydrate are two of the principal subsurface drilling hazards in deepwater. Shallow gas should be identified and avoided in the uppermost tophole section where casing is not set due to insufficient sediment strength. There is also increasing interest in evaluating the resource potential for concentrated gas hydrate sands. Whether there is subjacent gas under the gas hydrate deposits and their relative quantities is important to know when designing potential production strategies. In 2009, the Gulf of Mexico Gas Hydrate Joint Industry Project Leg II (JIP Leg II) drilled three Logging-while-drilling (LWD) sites to test the potential occurrence of gas hydrate in sandy sediments in Green Canyon 955 (GC 955). The LWD data allowed for the study of AVO for interpreting seismic amplitude anomalies on free-gas charged sands, hydrate-bearing sands, and hydrate-over-free-gas sands.

Although seismic amplitude is affected by many factors, AVO techniques have shown to be useful for direct hydrocarbon indication over the past three decades, especially for gas sand reservoir in the clastic depositional settings. In contrast, the application to identify shallow gas and gas hydrate has not reached the same level. Ecker et al. (1998) use rock physics-based AVO modeling to investigate the internal structure of hydrate-bearing sediments offshore Florida. Carcione and Tinivella (2000) compute AVO curves for consolidated Berea sandstone with gas hydrate and free gas. Furthermore, a few studies attempt to separate hydrate-bearing sediments (gas hydrate without free gas below) from hydrate-over-gas sediments (gas hydrate overlies free gas) from seismic amplitude; both are drilling hazards but different drilling strategies and protocols should be applied.

In Shuey's two-term approximation to the Zoeppritz equations, the P-wave reflection coefficient can be approximately written as a function with two parameters: AVO intercept (A) and AVO gradient (B) (Shuey, 1985). In general, deepwater sediments follow normal compaction processes, which define background trends. AVO anomalies can be observed from the crossplot of the intercept and gradient because they deviate from the background trend. Rutherford and Williams divided AVO anomalies into three categories (Classes I, II and III) based on normal incidence reflection coefficient (1989). Castagna and others proposed an additional category, Class IV, and presented the anomalies in terms of locations in the crossplot (Castagna et al., 1997 and Castagna and Swan, 1998). In this study, we investigate the AVO anomalies related to gas hydrate and/or free gas by simulating their AVO reflection coefficient responses and intercept and gradient in the A-B plane.

Geologic setting

The study area is at GC955 with water depths of 2,000-2,200 m, located on the middle continental slope in the northern Gulf of Mexico (Figure 1). The GC955 site is about 2,000-3,000 m southeast of the Green Canyon re-entrant on the base of the Sigsbee Escarpment (Figure 1). Shallow sediments are predominantly composed of hemipelagic fine-grained sediments in the Gulf of Mexico. However, there is a large submarine fan, the Mississippi Fan, which was deposited in the deepwater of the Gulf of Mexico during late Pliocene and Pleistocene in the shallow-section sediments at the GC955 site. Shelf-margin deltas were developed and channel-levee systems were deposited during sea level low stands. These channel-levee systems transported coarse-grained sediment from the continental margin to the slope via submarine canyons. When sea level rose during later geologic time, hemipelagic clays dominated the marine sedimentation in the area. Salt movement has generated numerous regional and local growth faults, which provide good migration paths for hydrocarbons. Under favorable conditions of temperature and pressure,

DOI http://dx.doi.org/10.1190/segam2012-1104.1

gas hydrate can form from thermogenic gas when migrating from the deep section into shallow section.

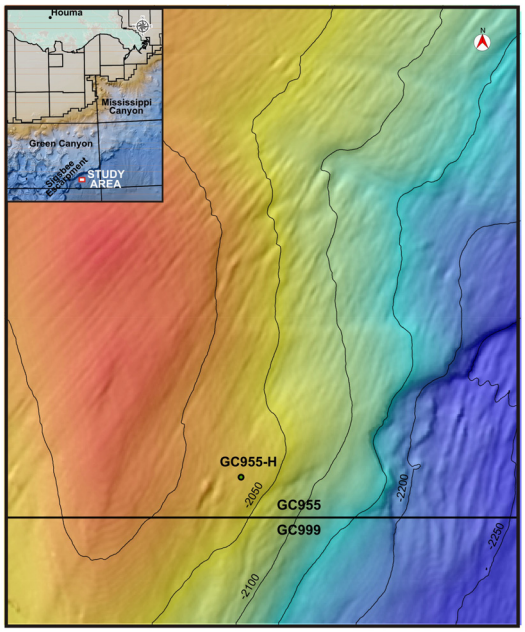

Figure 1: Shaded relief map shows the seafloor on GC955 and the relative location of well GC955-H.

Well log data

Figure 2 shows the Gamma Ray, Resistivity, Vp, and density logs measured from sites GC955-H.

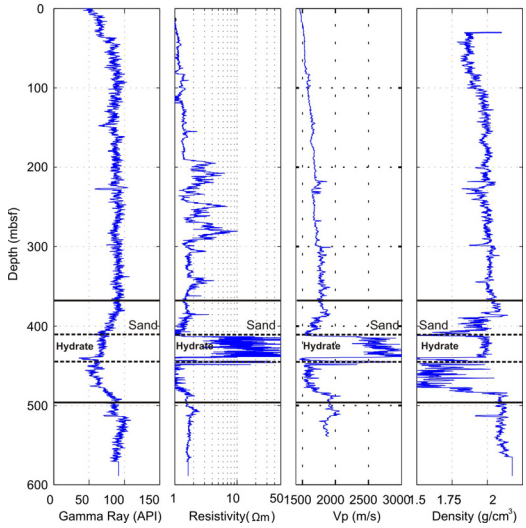

Figure 2: Gamma, resistivity, sonic, and density logs from well GC955-H.

Note the sharp increase of both resistivity and P-wave velocity in the well log display. Resistivity increases from 1 to 50 ohm-m and sonic velocity increases from about 1.6 km/s to 2.8 km/s between 410 and 450 mbsf. Gamma ray decreases from about 100 API to 50 API between 375 and 490 mbsf, indicating that highly-concentrated gas hydrate occurs in a sand section. The highest gas hydrate saturations estimated from resistivity logs in this section exceed 70% (Guerin et al., 2009). Figure 3 illustrates the crossplot of the P-wave velocity and Gamma Ray from portions of the logs in figure 2. The figure suggests that water-bearing sands have relatively lower velocities than clays, whereas hydrate-bearing sands are characterized by high velocities.

For the purpose of synthetic AVO modeling, P-wave velocity, S-wave velocity, and density of hydrate-bearing and free-gas-charged sands with respect to hydrate saturations were computed from rock physics model using the Hashin-Shtrikman bounds, Hertz-Mindlin contact theory, and Gassman fluid substitution. The computation was calibrated by measured log data and estimated hydrate saturation from resistivity logs.

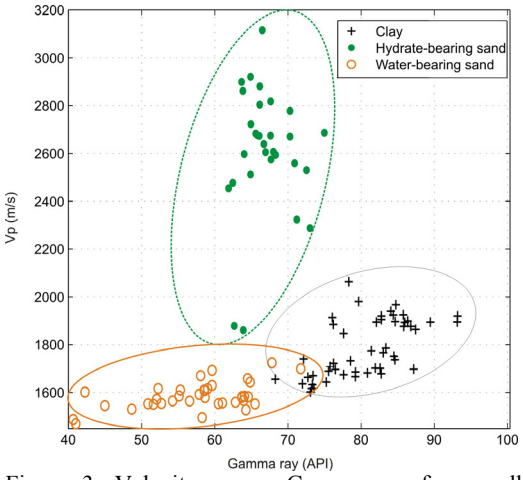

Figure 3: Velocity versus Gamma ray from well GC955-H.

AVO analysis

The goal of AVO analysis is to investigate reflection coefficient or amplitude responses on different sand models with respect to gas hydrate saturation and free gas saturation. The models are sufficiently constrained by well logs data and reasonable geologic environments. Although they may not precisely match real seismic data, synthetic AVO curves represent the effect of gas hydrate and free gas on seismic amplitude and provide guidance for plausible seismic explanations.

We computed synthetic AVO responses using the Shuey's approximation. The Vp and density of clay were extracted from well logs above gas hydrate reservoir. No S-wave velocity was available in the log data. S-wave

DOI http://dx.doi.org/10.1190/segam2012-1104.1

velocity is derived from density and shear modulus; the latter has been estimated and calibrated in our rock physics model. Thus, we used the model to reasonably predict the S-wave velocity. Similarly, the velocities and density of water-bearing, saturated hydrate-bearing, and free-gas-charged sands were computed from well logs and from the rock physics model.

Figure 4 shows the AVO responses with respect to gas hydrate saturation. The trends of reflection coefficient changes with angle of incidence are affected by the gas hydrate saturation. The AVO responses are weak for low saturation gas hydrate (25% gas hydrate saturation in figure 4), in which the reflection coefficients or amplitude slightly increase with increasing angle of incidence and the trend is relatively flat. As hydrate saturation increases, the slope of the reflection coefficient curves increases. The response of high saturation gas hydrate (75% gas hydrate saturation in figure 4) shows a clear AVO anomaly; it has low reflection coefficient in zero offset and then a steeply increasing reflection coefficient in middle and far offsets.

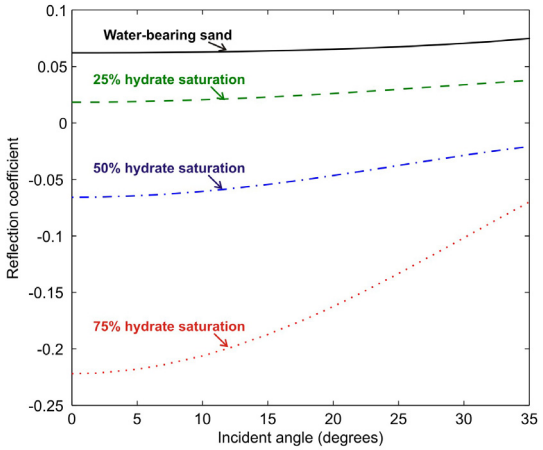

Figure 4: Variations of reflection coefficient with incident angle for different gas hydrate saturations in hydrate-bearing sands.

Figure 5 shows gas effect results in larger absolute reflection coefficients or amplitudes in hydrate over gas sands than hydrate bearing sands. The reflection coefficients decrease with the increasing angle of incidence for free-gas-charged sands and low saturated hydrate-over-gas sands, while the reflection coefficients increase with the increasing angle of incidence for high saturated hydrate-over-gas sands. For 40% saturated hydrate-over-gas sand, the reflection amplitude is near unity (Figure 5). This suggests that AVO anomalies first decrease with hydrate saturation increasing to a critical saturation, then, polarity reversal occurs, the anomalies increase with hydrate saturation increasing.

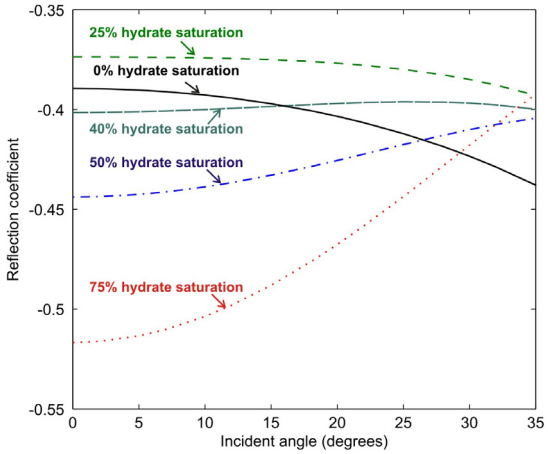

Figure 5: Variations of reflection coefficient with incident angle for different gas hydrate saturations in hydrate-over gas sands. 30% free gas saturation is assumed below hydrate layer in the sands.

AVO crossplot

The AVO classification presented by Rutherford and Williams (1989) and Castagna and Swan (1997) has become the industry standard for AVO analysis for oil and gas exploration. They classify gas sand responses into four classes. Class I is high impedance sand underlying low impedance shale and has a positive intercept and negative gradient for top of gas sand. Class II is small impedance contrast that the impedance of the sand is about the same as the overlying shale, the gradient is negative and the intercept may be negative or positive. Class III is low impedance sand underlying high impedance shale and amplitude increasing with offset; Class IV is also low impedance sand underlying high impedance shale but amplitude decreasing with offset. Thus the intercepts are negative for Class III and Class IV but the gradients are negative for Class III and positive for Class IV. We use the classification for hydrate-bearing sand and hydrate-over-gas sand. AVO intercept and gradient calculated from base of hydrate reflections and/or top of free gas reflections show in the crossplot plane.

AVO crossplot was designed to differentiate hydrocarbon-filling or other unusual sediments from background A versus B trends. Castagna and Swan indicate that the background trends pass through the origin and depend on Vp and Vp/Vs. The trends rotate toward the Y-axis for consolidated rock with Vp/Vs less than 2.5 while they rotate toward the X-axis for unconsolidated rock with Vp/Vs greater than 2.5.

DOI http://dx.doi.org/10.1190/segam2012-1104.1

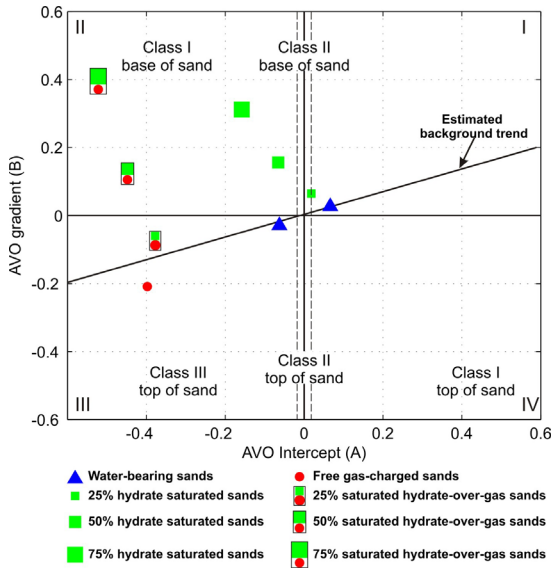

Figure 6: AVO crossplot of the modeled data.

In our model of unconsolidated sediments, the estimated background trend lies on the quadrants I and III that is consistent with their results (Figure 6). The AVO anomalies for hydrate-bearing sands are Class I or II, which are located in quadrants I and II. They show lower negative intercept and higher positive gradient for the higher hydrate saturations. This suggests that highly-concentrated hydrate-bearing sands may be clearly separated from water-bearing sands in the AVO crossplot.

Gas sand is typically Class III AVO. With increasing hydrate saturation at the top of free gas, AVO gradients generally increase and, then, are close to the background trends. Although the hydrate-over-gas sands exhibit Class IV behaviors, we do not emphasize the Classs IV AVO in figure 6 because it nears the estimated background trend and only small part of hydrate-over-gas sands below the trend in the quadrant III. On the other hand, Castagna and Swan define that Class IV should be in quadrant II in their paper (Castagna and Swan, 1997).

After crossing the background trend line (25% saturated hydrate-over-gas sand in figure 6), hydrate-over-gas sands move from quadrant III to quadrant II in the crossplot and show Class I anomalies. Higher concentrated hydrate exhibit more obvious Class I anomalies. Hydrate-over-gas sands have similar gradients with hydrate-bearing sands but much higher absolute intercept. In deepwater shallow section, the intercepts of A<-0.3 are considered as strong amplitude anomalies.

Conclusions

We have simulated and analyzed the AVO responses for hydrate-bearing sands, free-gas-charged sands, and hydrate-over-gas sands in deepwater environment. Our results indicate that the different AVO behaviors of these sediments are the consequence of different hydrate saturations and presence of free gas, and their interaction. Free gas-charged sands are Class III AVO while highly-concentrated hydrate-bearing sands and highly-concentrated hydrate-over-gas sands are Class I AVO anomalies. These AVO anomalies show apparent deviations from the background intercept versus gradient trend. Highly-concentrated hydrate-over-gas sands have very strong negative AVO intercept, which may suggest that highly-concentrated hydrate with free gas below can be separated from only highly concentrated hydrate sands. Thus, AVO analysis would be a useful tool for drilling hazard assessments to indicate the presence of gas hydrate and shallow gas in deepwater environment and for designing gas hydrate production strategies.

Acknowledgments

We would like to give special thanks to GoM Gas Hydrate JIP for providing the LWD log data from the Leg II field program.

http://dx.doi.org/10.1190/segam2012-1104.1

EDITED REFERENCES

Note: This reference list is a copy-edited version of the reference list submitted by the author. Reference lists for the 2012 SEG Technical Program Expanded Abstracts have been copy edited so that references provided with the online metadata for each paper will achieve a high degree of linking to cited sources that appear on the Web.

REFERENCES

Carcione, J. M., and U. Tinivella, 2000, Bottom-simulating reflectors: Seismic velocities and AVO effects: Geophysics, **65**, 54–67.

Castagna, J. P., and H. W. Swan, 1997, Principles of AVO crossplotting: The Leading Edge, **17**, 337–342.

Castagna, J. P., and H. W. Swan, and D. J. Foster, 1998, Framework for AVO gradient and intercept interpretation: Geophysics, **63**, 948–956.

Ecker, C., J. Dvorkin, and A. Nur, 1998, Sediments with gas hydrates: Internal structure from seismic AVO: Geophysics, **63**, 1659–1669.

Guerin, G., A. Cook, S. Mrozewski, T. S. Collett, and R. Boswell, 2009, Gulf of Mexico gas hydrate joint industry project leg II — Green Canyon 955 LWD operations and results: http://www.netl.doe.gov/technologies/oil-gas/publications/Hydrates/2009Reports/GC955LWDOps/pdf.

Rutherford, S. R., and R. H. Williams, 1989, Amplitude-versus-offset variations in gas sands: Geophysics, **54**, 680–688.

Shuey, R. T., 1985, A simplification of Zoeppritz equations: Geophysics, **50**, 609–614.